NRIAG Journal of Astronomy and Geophysics 6 (2017) 5–18

Contents lists available at ScienceDirect

NRIAG Journal of Astronomy and Geophysics

journal homepage: www.elsevier.com/locate/nrjag

Full length article

Atmospheric conditions affecting seeing at St. Catherine: Estimation of operational time for NRIAG new telescope☆

Sayed A. Mekhaimr

National Research Institute of Astronomy and Geophysics, Cairo, Egypt

ARTICLE INFO

Article history:
Received 8 January 2017
Accepted 13 April 2017
Available online 16 June 2017

Keywords:
Climate
Seeing
Astronomical observation
New telescope site test

ABSTRACT

The study of the prevailing atmospheric conditions is an essential part of any site testing for a new telescope establishment. In this article, the meteorological parameters that affect the *astronomical seeing* at St. Catherine region, where a two candidate sites are located, are studied based on the available climate data. The complex topographical features of the region cause some differences between the weather at the nearest meteorological station and that at the candidate sites. This issue is illustrated through high resolution atmospheric modeling for short period (six days) as a case study. Finally, a preliminary estimation of operational hours for the telescope at the candidate sites is calculated.

1. Introduction

The increase of light pollution over the last three decades from Greater Cairo had bad impacts on the operation of Kottamia observatory, as observed by Asaad and Morcos (1982) and Nawar et al. (1995). Also, the nearby megaproject of *New Administrative Capital* will end the excellence of the largest telescope in the North Africa and Middle East. Therefore, the National Research Institute of Astronomy and Geophysics (NRIAG) decides to build a new large telescope in Uninhabited region, which is supposed to be faraway from any urban communities during the twenty-first century. This paper discusses the atmospheric conditions that affect the *astronomical seeing* at two of candidate sites, that are located near the Saint Catherine Region in south of Sinai.

The astronomical observation quality (*seeing*) for a new telescope at any candidate site depends mainly on the prevailing meteorological conditions at the site. Atmospheric parameters like cloud cover, relative humidity, wind, atmospheric turbulence, precipitation, raising sand, dust storm, haze, mist and fog, have direct effects on the astronomical observation quality. These parameters and some other parameters (e.g. temperature and flash flood) should also play a role in the construction design of the telescope, the dome and other associated buildings in the site, in order to obtain the best operation and comfort environment (e.g. ventilation, avoiding cold or heat stress, energy consumption).

The studies of the atmospheric conditions for new large telescopes are an essential part of any site test. These studies include the climatology of the candidate sites (e.g. Lombardi et al., 2009; Varela and Muñoz-Tuñón, 2009) and the relation between the meteorological observations and seeing measurements by using a differential image motion monitor; *DIMM* (e.g. Erasmus, 2000; Bradley et al., 2006). Also, these studies are an important part for the *adaptive optics*. Recently, the *optical turbulence* attracts a lot of attention and the prediction of its 3D maps became a new trend in the modern ground based astronomy (Masciadri and Sarazin, 2009). This prediction is mainly done by using high resolution atmospheric modeling (Masciadri et al., 1999a,b).

The paper begins in Section 2 with a list of the data sets used in the present work. The topographical complexity of the region makes a big difference in a micro-climate form one site to another, in the same region. So, in Section 3, the topographical features of the candidate sites and their effects on the micro-climate are discussed. Beginning from Section 4 till Section 9 the climatology of the atmospheric variables that affect the astronomical observations are analyzed; cloud Cover, relative humidity, precipitation, wind, and some phenomena related to visibility (mist, haze, raising sand, dust storm). These analyses are based on available climate data from just one meteorological station, which is located at Saint Catherine airport. Actually, this station does not necessary

☆ Part of this work is included in unpublished internal report: Sayed Mekhaimr, Preliminary Report on St. Catherine Climatology as part of Site Test for New NRIAG Telescope, NRIAG, 2017.

E-mail address: mekhaimr@nriag.sci.eg

Peer review under responsibility of National Research Institute of Astronomy and Geophysics.

Production and hosting by Elsevier

http://dx.doi.org/10.1016/j.nrjag.2017.04.005

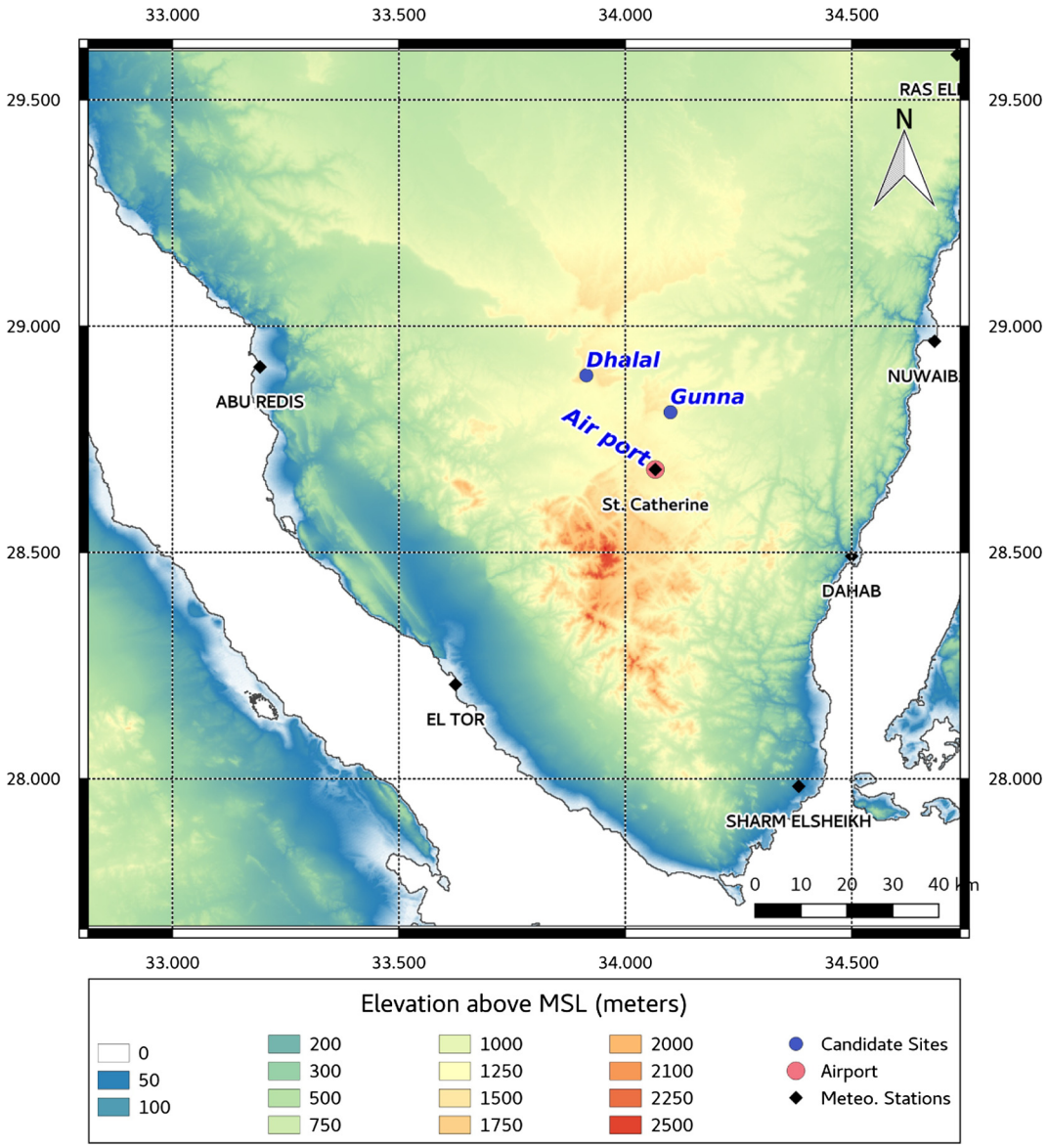

Fig. 1. South Sinai topography.

represent the atmospheric condition for the candidate sites as a result of topographical complexity. That is why there is a need for high resolution modeling for long period (at least one year), which will be done in the future work. However, in Section 10, a high resolution modeling for a case study (six day simulation) is used to emphasize the weather differences at the candidate sites and that at the available meteorological station. In Section 11 a preliminary estimation of the missing hours (nights) are made based on the analysis of the climatology of all previous variables. Finally, in Section 12 some concluding remarks are outlined.

2. Data sets

In the south part of Sinai, there are six meteorological stations indicated by black dots in Fig. 1. Five of them are near the coats and only St. Catherine meteorological station is representing the mountain region. Also, all these stations, except St. Catherine, are far from the candidate sites. For these reasons St. Catherine meteorological station is chosen to study the climatology of the candidate sites.

The Saint Catherine meteorological station (WMO ID:62457) is located at the airport with coordinates: 28°41′N and 34°4′E, and elevation 1350 m above mean sea level (MSL). This station records the atmospheric conditions since Nov 1979.[1] This work uses the following data sets about St. Catherine meteorological station:

- DS01: Climate Normals during (1981–2010) (EMA),[2]
- DS02: Climate data for year 2015 (EMA),[3]
- DS03: Wind Direction and Speed Frequencies for year 2012 (EMA),[3]
- DS04: Hourly Data during March 2012 to Dec 2016 (METAR reports),[4]
- DS05: Climate Normals during (1961–1990) (NOAA).[5]

3. Topographical features

The central part of South Sinai has a complex terrain. It is mountainous region, with the highest summit in Egypt (Mount Cather-

[1] The old meteorological St. Catherine station had another location.
[2] Under publication.
[3] Data is obtained by request from EMA.
[4] https://mesonet.agron.iastate.edu.
[5] ftp://ftp.atdd.noaa.gov/pub/GCOS/WMO-Normals/RA-I/UB/62457.TXT.

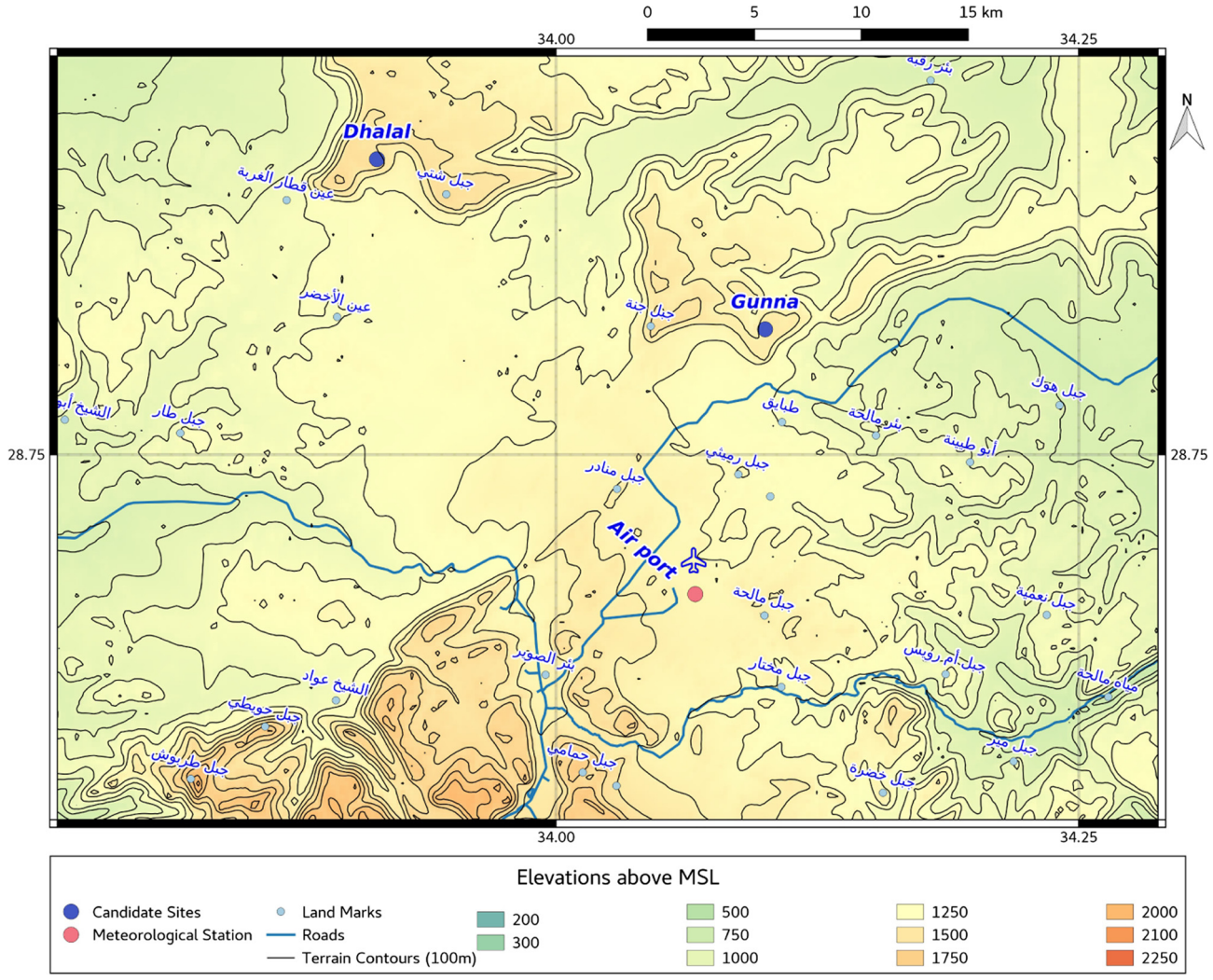

Fig. 2. Topography complexity near St. Catherine meteorological station and two candidate stations.

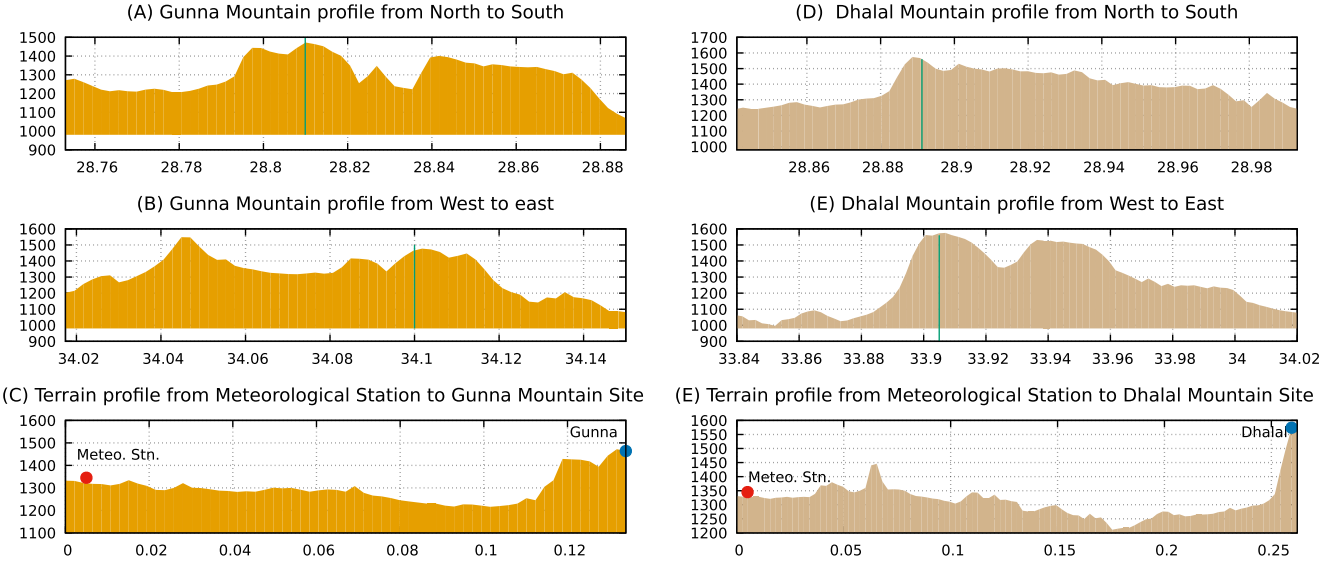

Fig. 3. Terrain features of two candidate sites: Gunna (left column) and Mt. Dhalal (column right).

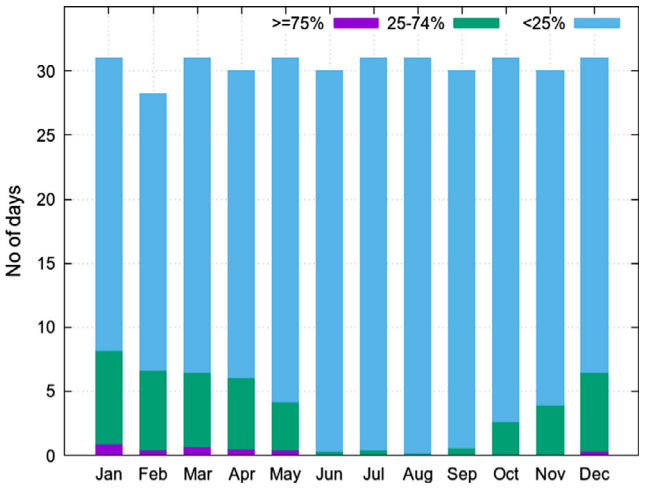

Fig. 4. Monthly number of occurrences for three categories of cloud cover; clear sky (<2 oktas) light blue, partly cloud (3–5 oktas) green, cloudy sky (⩾6 oktas) violet. during 1981–2010.

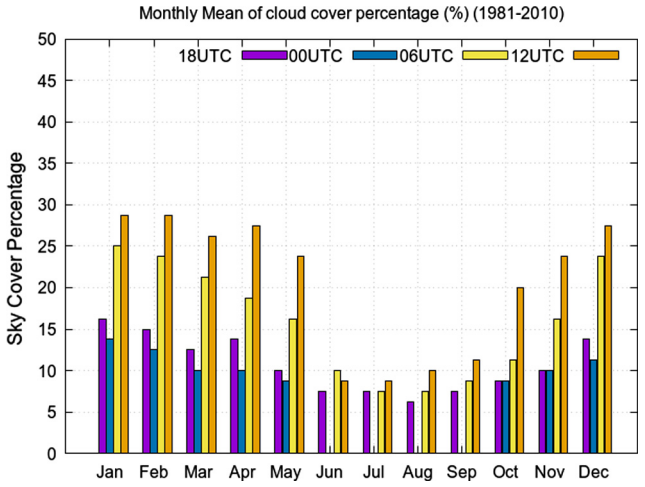

Fig. 5. Monthly mean of cloud cover at 0, 6, 12, 18 UTC. during 1981–2010.

ine; 2629 m). The southern part of the region is composed of igneous rocks, with sharp edges and there are many valleys and canyons. When a dense rain falls on these mountains, it may drain toward the gulf of Suez or the Gulf of Aqaba. In the northern part of the region, there is *El-Tih plateau*, which is a limestone plateau, it gradually slopes from south to north toward the Mediterranean.

Fig. 1 shows the topographical features of South Sinai and the location of Saint Catherine airport, which is indicated by the red dot, and the two candidate sites are indicated the blue dots. These sites are

- Gabel Dhalal:
  - Lat: 28°53′28.4″N
  - Lon: 33°54′51.6″E
  - maximum elevation: 1606 m
  - distance from airport: about 15 km.
- Tel Gunna:
  - Lat: 28°48′35.7″N
  - Lon: 34°06′E
  - maximum elevation: 1589 m
  - distance from airport: 29 km.

Table 1
Number of occurrences of cloudy or partly cloudy sky (> 25%).

GMT	Jan	Feb	Mar	Apr	May	Jun	Jul	Aug	Sep	Oct	Nov	Dec	LCT
0	2.7	1.2	1.9	1.3	0.0	0.0	0.0	0.0	0.0	0.9	0.9	1.8	2
1	2.5	1.2	1.4	0.3	0.5	0.0	0.0	0.0	0.0	0.7	0.9	1.2	3
2	2.2	1.5	1.4	0.5	0.2	0.0	0.0	0.0	0.0	1.2	0.7	1.1	4
3	2.6	1.5	1.3	1.8	0.7	0.0	0.0	0.0	0.2	0.9	0.7	1.6	5
4	3.2	2.1	1.7	2.1	0.7	0.0	0.0	0.0	0.2	0.9	1.4	2.7	6
5	3.2	2.6	1.1	1.5	0.7	0.0	0.2	0.0	0.2	1.6	2.0	4.1	7
6	5.1	3.2	2.2	1.9	0.9	0.2	0.2	0.0	0.2	1.4	2.4	4.7	8
7	5.9	3.6	2.6	1.4	1.2	0.2	0.5	0.0	0.2	1.1	3.5	5.5	9
8	6.5	3.9	3.5	1.6	1.1	0.2	0.2	0.0	0.2	1.6	3.5	5.9	10
9	8.2	4.2	1.9	2.9	2.1	0.4	0.7	0.5	2.6	3.7	5.6	11
10	7.2	4.4	2.4	3.7	2.3	0.6	2.8	1.1	0.5	3.8	4.7	5.3	12
11	8.0	4.5	2.9	5.9	4.4	0.9	3.6	1.3	1.2	6.0	5.3	6.9	13
12	9.4	4.8	3.3	6.2	6.0	1.7	5.4	2.2	1.9	6.2	5.8	6.6	14
13	9.9	5.5	3.7	6.5	7.0	2.6	5.4	3.7	2.6	8.0	6.7	6.5	15
14	8.9	5.6	4.5	7.0	6.4	2.2	5.0	4.4	3.5	8.3	7.1	6.7	16
15	8.3	4.6	4.3	6.4	5.7	2.1	5.7	4.6	3.9	7.8	6.7	5.3	17
16	6.9	5.1	4.3	5.6	4.0	1.9	5.7	4.0	2.5	5.4	5.4	5.2	18
17	6.0	3.3	3.5	5.7	3.1	0.9	3.0	2.0	1.9	2.9	3.5	4.9	19
18	4.6	1.8	2.2	2.9	1.7	0.2	1.4	0.6	1.1	1.3	2.7	2.9	20
19	4.1	1.5	1.9	1.8	1.3	0.2	0.5	0.7	0.5	0.9	2.4	2.5	21
20	3.0	1.2	1.7	1.3	0.7	0.2	0.0	0.4	0.5	1.1	1.3	1.8	22
21	2.4	1.1	1.3	1.0	0.2	0.0	0.0	0.2	0.5	0.7	0.9	1.9	23
22	3.0	1.1	1.1	0.6	0.2	0.0	0.0	0.0	0.5	0.5	0.9	1.8	0
23	2.4	1.1	1.6	1.0	0.0	0.0	0.0	0.0	0.2	0.7	1.1	1.6	1
Night	3.0	1.4	1.6	1.5	0.7	0.1	0.4	0.4	0.5	1.0	1.4	1.9	Sum = 13.9

These two sites are located at Egma plateau (the south-most of El-Tih plateau), while the meteorological station is located at the airport, which exists in the north-east of the Sinai mountains. The topography complexity near candidate sites are shown in Fig. 2, which reflects many valleys, canyons and highlands.

These irregular terrain features have direct effects on the local climate and they make a large variability in the climate from one site to another. For example, St. Catherine meteorological station is located at relatively low flat land surrounded by a high mountain from the south-west, which causes the atmospheric flow in the boundary layer to be aligned with the terrain and there is relatively no south wind or south-east wind (see Section 8). Since the two candidate sites are about 200 meters higher than the location of the meteorological station, then they are expected to be colder by one or two degrees than the station by assuming dry lapse rate, but in some weather conditions Dhalal site become colder by four degrees than the station (see Section 10). The diurnal variation of wind will be different from that recorded by the station due to the locations of the two sites on the summits of mountains while the station is located in valley. in addition, the different sites have different rainfall amounts. These differences are will be illustrated in the case study (Section 10).

The terrain configurations of the candidate mountains are depicted in Fig. 3, which illustrates the terrain profiles from North to South, from West to East, and the cross section terrain profiles between each candidate site and the meteorological station's location. The terrain profile shape plays an important role in the atmospheric flow stream around or above the mountain. Also, it has direct effect on the diurnal variation of mountain-valley circulation. For example, if the atmospheric flow goes over the mountain, the gravity waves will be generated, which are associated with clouds and atmospheric turbulence. The turbulence will cause perturbations in the refractive index, and distortions in the astronomical imaging. Therefore, it is recommended to put telescope in mountain side facing the prevailing wind in the region, because the turbulence occurs in the lee side (for more details see Stull, 1988; Whiteman, 2000; Barry, 2008).

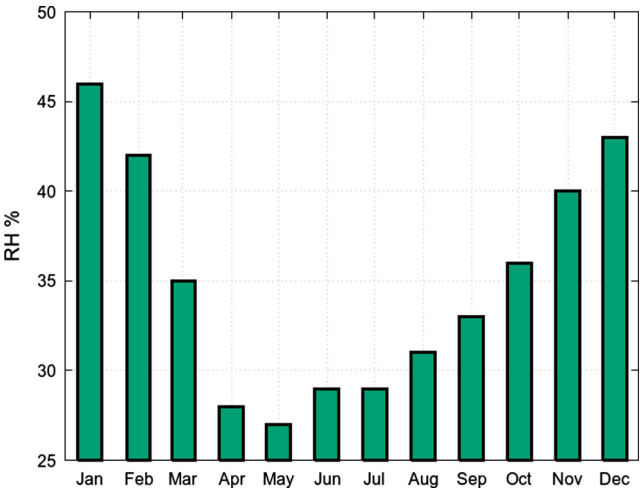

Fig. 6. Relative humidity climate normals (1981–2010).

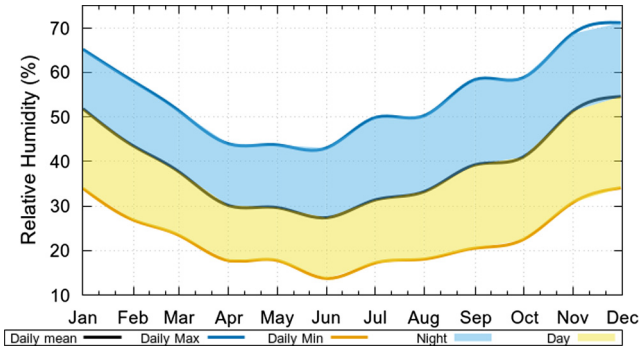

Fig. 7. Monthly mean relative humidity during (Mar 2012–Dec 2016).

Table 2
Number of occurrences for relative humidity > 75%.

GMT	Jan	Feb	Mar	Apr	May	Jun	Jul	Aug	Sep	Oct	Nov	Dec	LCT
0	11.5	7.9	5.2	1.5	0.9	0.0	0.0	0.7	2.3	4.2	12.3	13.8	2
1	10.6	6.1	5.2	1.8	1.1	0.4	0.0	0.2	2.8	5.2	12.7	15.0	3
2	12.2	9.0	5.4	2.3	1.6	1.1	1.1	0.5	4.5	6.6	13.0	16.8	4
3	12.3	8.3	4.9	2.5	1.3	1.3	0.9	0.2	5.5	6.6	12.7	14.2	5
4	11.4	8.0	5.0	1.8	0.7	0.4	0.2	0.5	4.8	6.4	12.2	14.4	6
5	11.0	5.8	2.2	0.9	0.2	0.0	0.0	0.0	2.0	4.2	8.7	12.2	7
6	8.2	4.4	2.2	0.3	0.2	0.0	0.0	0.2	0.0	0.5	4.1	6.5	8
7	5.4	1.2	0.8	0.0	0.0	0.0	0.0	0.0	0.2	0.0	0.4	5.3	9
8	2.6	0.3	0.5	0.0	0.0	0.0	0.0	0.0	0.0	0.0	0.2	1.4	10
9	3.1	0.9	0.3	0.0	0.0	0.0	0.0	0.0	0.0	0.0	0.2	0.9	11
10	2.0	0.3	0.3	0.0	0.0	0.0	0.0	0.0	0.0	0.0	0.2	0.0	12
11	1.7	0.3	0.3	0.0	0.0	0.0	0.0	0.0	0.0	0.0	0.0	0.2	13
12	1.4	0.6	0.3	0.0	0.0	0.0	0.0	0.0	0.0	0.0	0.0	0.4	14
13	1.4	0.3	0.3	0.0	0.0	0.0	0.0	0.0	0.0	0.0	0.0	0.7	15
14	1.1	0.6	0.3	0.0	0.0	0.0	0.0	0.0	0.0	0.0	0.0	0.7	16
15	1.7	0.0	0.5	0.0	0.0	0.0	0.0	0.0	0.0	0.0	0.7	0.7	17
16	2.6	0.9	0.3	0.0	0.0	0.0	0.0	0.0	0.0	0.0	0.6	0.9	18
17	3.8	1.5	0.8	0.0	0.0	0.0	0.0	0.0	0.0	0.0	0.9	1.8	19
18	5.1	2.1	0.3	0.0	0.0	0.0	0.0	0.0	0.5	0.0	2.1	4.7	20
19	8.2	2.7	0.6	0.0	0.0	0.0	0.0	0.0	0.0	0.7	3.9	7.0	21
20	9.7	2.7	1.1	0.3	0.2	0.0	0.0	0.0	0.2	1.1	5.7	9.1	22
21	10.2	4.9	1.3	0.0	0.4	0.0	0.0	0.2	0.7	1.4	7.9	9.5	23
22	11.3	4.9	3.3	0.0	0.7	0.0	0.0	0.0	1.2	2.7	9.9	9.8	0
23	11.7	6.6	3.5	0.3	0.2	0.2	0.0	0.4	1.8	3.9	10.0	12.2	1
Night	10.1	5.2	2.9	0.7	0.6	0.2	0.1	0.2	1.6	2.9	8.6	10.9	Sum = 43.8

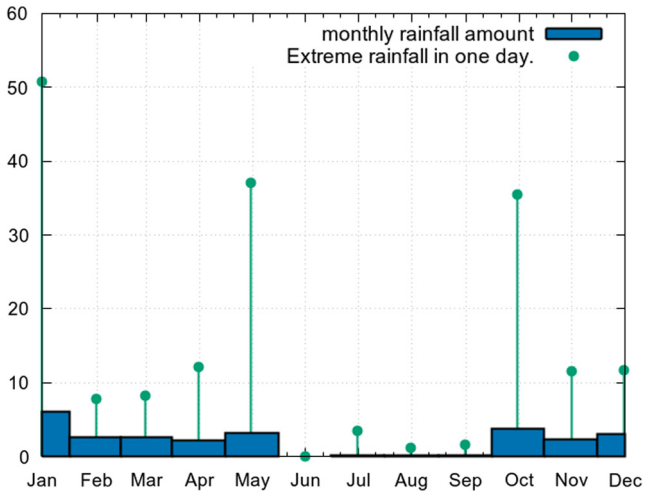

Fig. 8. Mean of rainfall amount (kg/m^2) and extremes (1981–2010).

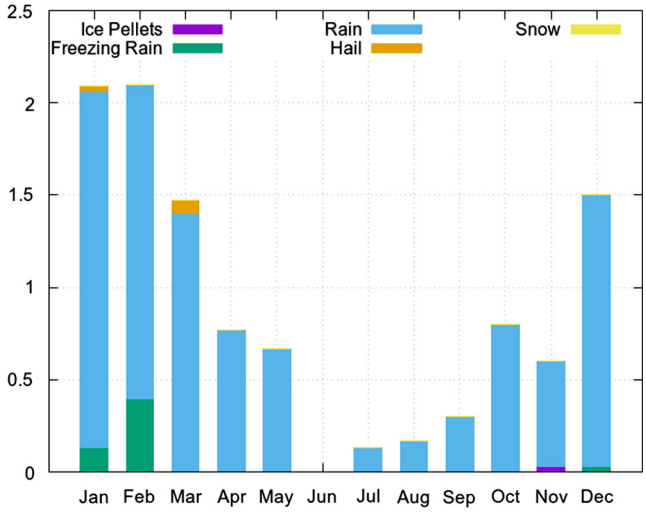

Fig. 9. Mean of numbers of days of precipitations (1981–2010).

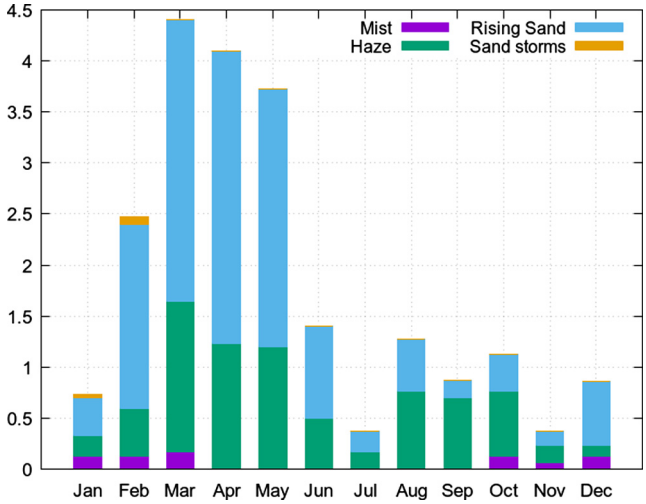

Fig. 10. No. of days of visibility related phenomena (1981–2010).

4. Cloud cover

The cloud cover has a direct impact on the astronomical observations. The best observation conditions occur in the clear sky days (No clouds or very few clouds). According to WMO, *the total cloud cover is defined as the fraction of the celestial dome covered by all the clouds visible* (WMO, 1975). The observer divides celestial dome

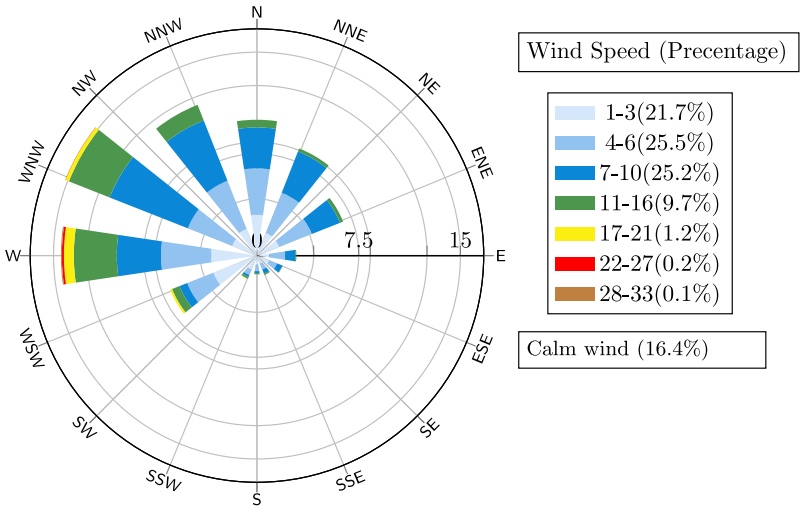

Fig. 11. Annual wind rose 2012.

into eight sections (called *oktas*), and then estimates how many oktas is covered by clouds.

Fig. 4 shows the monthly mean of number of occurrence for three Categories of cloud cover:

- clear sky or few clouds (<2 oktas),
- partly cloud (3–5 oktas), and
- cloudy sky ($\geqslant 6$ oktas).

Fig. 4 is drawn by using the climate normals during 1981–2010 [DS01]. This figure shows the number of occurrences for three categories of cloud cover; clear Sky (<2 oktas) light blue, partly cloud (3–5 oktas) green, cloudy sky ($\geqslant 6$ oktas) violet. The figure indicates that *St. Catherine site has a clear sky most of the year (about 319 days), The maximum number of cloudy sky days occur in winter (Nov., Dec., Jan., Feb.) and spring (Mar., Apr., May.), while June, July and August have a clear sky.*

The diurnal variation of cloud amount can be shown by using climate normals of clouds amount during (1981–2010) at four times 00 UTC, 06 UTC, 12 UTC, 18 UTC (see Table 8). In addition, Fig. 5 shows that the most of cloud amount occurs at local noon time (12 UTC), while the minimum occurs after mid-night (00 UTC). The mean cloud cover during winter and spring is about 25% in day time and 12% at nighttime, while in summer the mean cloud cover does not increase more than 10% in day time, and the night has no cloud.

In order to estimate the best hours for astronomical observations, the hourly data [DS04] should be used. Actually DS04 data set covers period from March 2012 to Dec 2016, which is a short period from a climate point view, but it still useful for our calculation. By using these hourly data, Table 1 is made. It shows the number of occurrences for cloudy or partly cloudy sky ($>25\%$) during 24 hours at different months. These numbers are colored according to their values; the times with large numbers are colored with blue, while small values are colored with light blue, and zero value has no color. By using this color gradient table, anyone can easily determine the best hours for astronomical observations in each month, where these hours correspond to cells with no color or light blue.

By assuming that nighttime begins at 7 PM and ends at 5 AM (local time), the mean number of nights of cloud cover more than 25% are given in the last row in Table 1. which indicates that *the total number of missing night due to cloud cover is approximately 14 nights.*

5. Relative humidity

The increase of relative humidity above a critical value will reduce the atmospheric transmission, which will affect the astronomical observations. Where the scattering, absorption and re-radiation of light by water vapor suspended particles will increase the sky brightness near infrared band at night (Bradley et al., 2006). Moreover, the increase of relative humidity grater than 75%, will increase the probability of water vapor condensation over the optics parts of telescope, which may cause oxidation, leaching, and eventual delamination the of optical coatings (Bradley et al., 2006).

According to the climate Normals during (1981–2010) [DS01], St. Catherine site is more humid in winter season (Nov, Dec, Jan, Feb) and more dry in spring and summer, as shown in Fig. 6.

Fig. 7 shows the monthly mean of daily maximum, minimum, and mean of relative humidity during (Mar 2012–Dec 2016), based on data set [DS04]. From this figure it is obvious that the night-time is more humid than the day-time, and winter is more humid than summer. The diurnal variation of mean relative humidity is about 30%, while the season variation of the mean is about 20%.

Table 2 shows the monthly mean of number of occurrences for observations of relative humidity greater than or equal 75% during the 24 hours. The table cells are colored according to their values, where the hours of larger number of occurrences have green color, while the hours of lower values have light green.

The last row in Table 2 illustrates the mean number of nights of relative humidity greater than or equal to 75%. Which indicates that *the number of missing nights due to high humidity is about 44.*

6. Precipitation and flood

The precipitation has contradictory impacts in the atmospheric observations, where during the precipitation periods, it is impossible to make any astronomical observations, but the precipitation wash out the air from any suspended aerosols; therefore after some rain cases, where all clouds are discharged and it becomes a stable weather, one can get the best condition for seeing.

The climate normals of St. Catherine station indicates that it has a little amount of precipitations (compared with the north coastal region of Sinai). The annual amount in St. Catherine is about 26.3 mm. But there were some extreme precipitation events over St. Catherine where the rainfall reached up to 50 mm per one

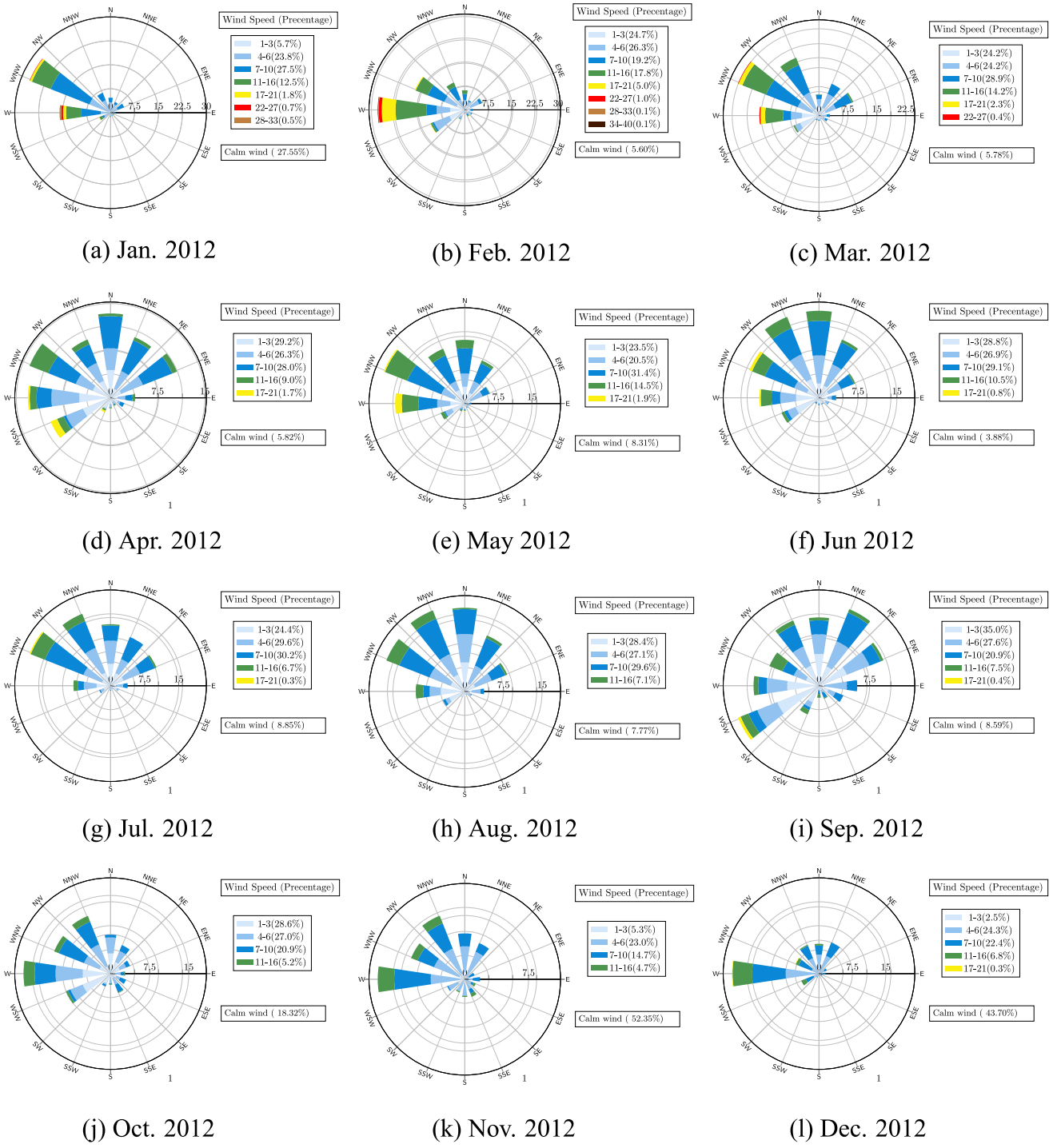

Fig. 12. Monthly wind rose.

day. This extreme event is a flood event, which might cause damages in buildings; therefore it should be considered in the telescope's dome design.

Fig. 8 shows the monthly mean of precipitations and the extreme rainfall based on climate data during (1981–2010) [DS01]. This figure indicates that summer season is free of precipitations, except some rare events with very small amount. Fig. 9 illustrates that the number of precipitations events (rainfall, freezing rain, hail, and ice pellets). Where *The annual number of precipitations events are about 11 events.*

7. Phenomena affect visibility

The astronomical observation is badly affected by some weather phenomena like sand storms, raising sand, haze, mist and fog. These phenomena reduces the horizontal visibility to less than 10 km and it may reach few meters in some cases.

Fig. 10 illustrates the number of these phenomena at St. Catherine site. The most frequent phenomena is the raising sand and haze. The maximum number of these phenomena occurs in spring due to Khamaseen depression. There is no fog is recorded during

Table 3
Number of times of wind speed greater than 15 km/h.

GMT	Jan	Feb	Mar	Apr	May	Jun	Jul	Aug	Sep	Oct	Nov	Dec	LCT
0	3.6	2.6	1.4	0.5	0.7	0.0	0.0	0.0	0.0	0.0	0.2	0.9	2
1	2.8	1.8	1.1	0.8	0.7	0.2	0.0	0.0	0.0	0.0	0.2	0.9	3
2	2.5	2.1	1.4	0.5	0.7	0.2	0.0	0.0	0.2	0.0	0.0	0.7	4
3	2.6	3.2	1.6	1.0	0.4	0.2	0.0	0.0	0.0	0.2	0.0	0.4	5
4	2.3	2.7	1.4	1.5	0.5	0.2	0.0	0.2	0.0	0.0	0.0	1.6	6
5	2.7	2.0	0.8	1.7	0.5	0.0	0.0	0.0	0.0	0.2	0.0	0.9	7
6	3.4	1.8	2.2	2.5	0.7	0.4	0.2	0.5	0.5	0.2	0.0	0.7	8
7	3.1	2.4	3.4	3.2	2.1	0.7	0.2	0.5	0.5	0.2	0.0	2.0	9
8	3.7	5.1	3.0	4.6	3.8	1.6	0.5	0.7	0.5	0.2	0.4	2.0	10
9	3.7	5.4	4.5	4.7	5.0	1.5	2.2	1.3	2.3	1.2	0.4	1.5	11
10	3.3	4.7	5.3	3.7	5.9	4.5	2.1	2.7	3.7	1.2	1.4	2.9	12
11	4.6	4.8	6.8	6.8	5.8	4.1	1.9	1.8	3.0	1.4	2.2	2.9	13
12	5.3	4.2	7.6	7.7	7.8	4.7	3.2	4.5	5.2	2.1	1.8	2.4	14
13	4.7	5.5	6.8	8.2	8.8	5.8	3.8	5.5	4.5	3.4	1.3	3.0	15
14	4.7	5.7	6.4	8.3	8.6	6.1	3.3	3.3	4.2	3.0	1.1	2.6	16
15	4.2	4.3	5.1	7.6	7.8	6.7	7.0	4.6	4.6	3.2	0.9	2.0	17
16	2.9	3.6	3.2	5.0	6.5	4.3	4.6	4.9	3.0	1.6	0.6	2.0	18
17	2.7	2.4	1.9	3.4	3.6	1.5	2.8	2.8	1.6	1.1	0.7	1.3	19
18	3.5	2.4	0.8	0.9	2.0	1.1	1.4	1.7	0.9	0.2	0.6	1.1	20
19	2.7	2.4	0.8	1.6	1.3	0.7	1.2	0.4	0.0	0.2	0.0	1.5	21
20	2.7	3.3	0.8	0.5	1.1	0.4	0.0	0.0	0.0	0.0	0.2	1.1	22
21	1.9	1.7	1.6	0.5	0.9	0.0	0.5	0.0	0.2	0.2	0.4	1.6	23
22	2.7	2.0	1.7	0.3	0.2	0.0	0.5	0.0	0.0	0.2	0.0	1.1	0
23	2.7	2.0	1.1	0.3	0.0	0.2	0.0	0.0	0.0	0.5	0.0	1.1	1
Night	2.8	2.2	1.2	0.6	0.8	0.3	0.4	0.2	0.2	0.2	0.2	1.1	Sum = 10.2

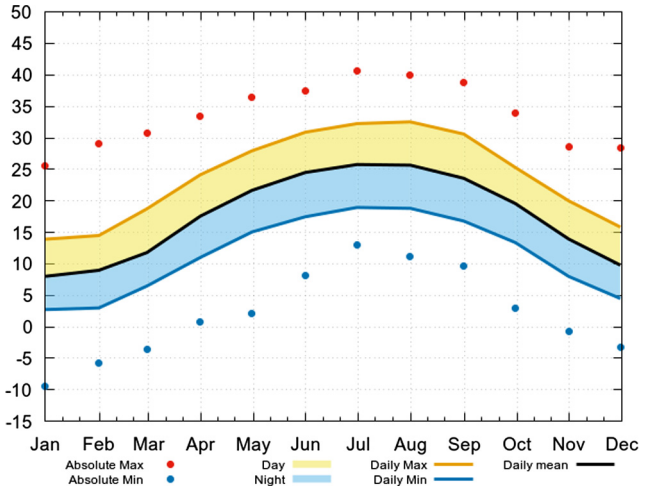

Fig. 13. Monthly mean temperature, daily maximum, and minimum, and extreme minimum and maximum temperature (1981–2010).

30 years (1981–2010). Mist requires a relative humidity $> 75\%$ and stable weather which may occur at night-time and early morning in winter, while raising sand and dust storm require high wind speed, which usually occurs in St. Catherine afternoon. The suspended dust particles due to raising sand and dust storm do not necessary fall down at night, so they affect the astronomical imaging at night.[6]

Table 9 tells us that *The total number of missing days due to these phenomena is about 22 days.*

8. Wind

The increase of wind speed may decrease the seeing quality and best astronomical imaging can be obtained under light wind (Bradley et al., 2006). Where the increase of wind speed implies the increase of wind shear and atmospheric turbulence. Moreover, the wind speed increase may be associated with the occurrence of raising sand or dust storm, which prevents astronomical observations.

The prevailing wind in Saint Catherine is West and North-West as seen from Fig. 11. Which shows the annual wind rose for year 2012, based on data set [DS03]. From this figure it obvious that there is no wind coming from east or south-east due to the topography around the meteorological station.

There are seasonal variation of wind directions and speed, where in winter and spring the wind speed is larger and has west and west north directions. While in summer the wind speed has low values and the wind directions are more variable (see Fig. 12).

Diurnal variation of wind speed in Saint Catherine can be shown by Table 3, where the wind speed increases in daytime and decreases at nighttime. The most times of wind speed greater than or equal to 15 km/h occur after noon (between 13 and 17 local time). The number of windy nights with wind $\geqslant$ 15 km/h is given in the last row of the table. Thus, the annual number of missing nights due to windy weather may be around 10 days.

Table 4
Estimated no. of nights with $T \leqslant 0$ °C for the candidate sites.

GMT	Jan	Feb	Mar	Apr	May	Jun	Jul	Aug	Sep	Oct	Nov	Dec	Sum
Night	7.4	2.0	0.1	0.0	0.0	0.0	0.0	0.0	0.0	0.0	0.0	2.7	12.2

9. Temperature

The temperature has no direct effects on the astronomical observations, but the spatial and temporal temperature gradient play an important role in enhancing the atmospheric turbulence, which degrades the seeing.

Fig. 13 shows the monthly mean of daily mean, minimum, and maximum temperature, besides the extreme minimum and maximum temperature for St. Catherine station, which is 1350 m above ground. This figure is based on climate normals (1981–2010) [DS01].

In winter nights, when the temperature approaches 0 °C the dew may be formed on any solid surface and there is a dangerous to the telescope optics. So it is important to calculate the number of times which have temperature less than or equal 0 °*C* for the candidate sites.

Since the candidate sites are above the altitude of meteorological station by about 200 m, then the temperature of these sites will be colder than meteorological station by two degrees under the assumption of *dry adiabatic lapse rate*, 1°/100 m. Thus by using data set (DS04) (March-2012 to Dec 2016) the number of missing hours due to temperature is calculated and the results is given in Table 4. Which illustrates that The total number of nights with temperature less than or equal 0 ° C for the candidate sites is about 12 nights.

10. High resolution modeling (case study)

Atmospheric numerical simulation for period from 0 UTC on 12 Feb. 2014 to 0 UTC on 18 Feb. 2014 has been made by using Weather Research and Forecasting model (ARW–WRF) (Skamarock et al., 2008), with three nested domains, with resolutions (30 km, 10 km, 2 km), as shown in Fig. 14. This simulation is driven by FNL NCEP reanalysis (1 deg resolution) as initial and boundary conditions (NCEP, 2000).

[6] The meteorological observers may not observe these suspended particles at night, especially when the horizontal visibility is more than 10 km, so the number of hazy atmosphere may be under estimation.

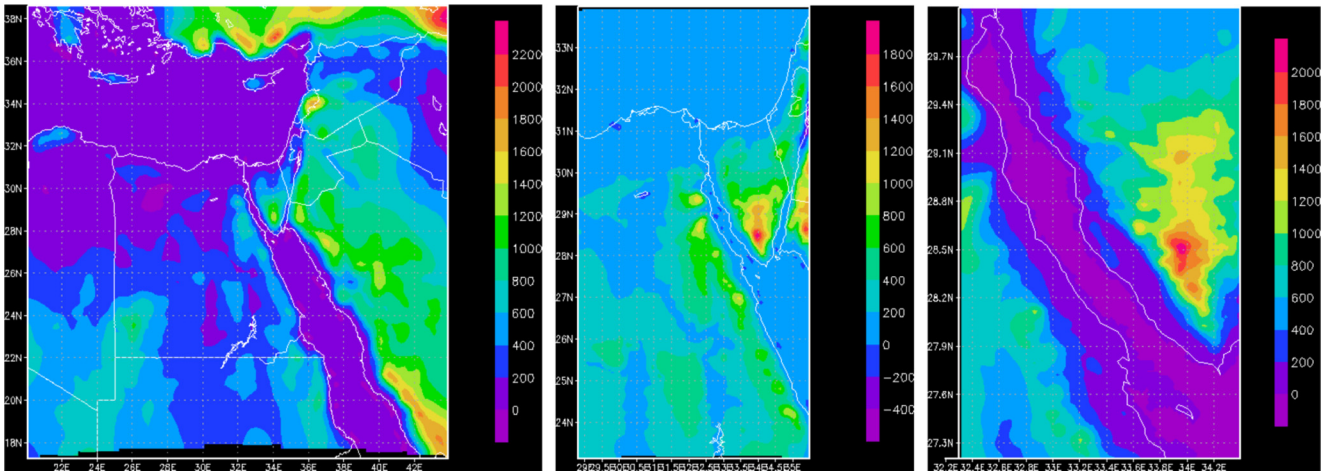

Fig. 14. The topography representations in three nested domains: left (30 km), middle (10 km), right (2 km).

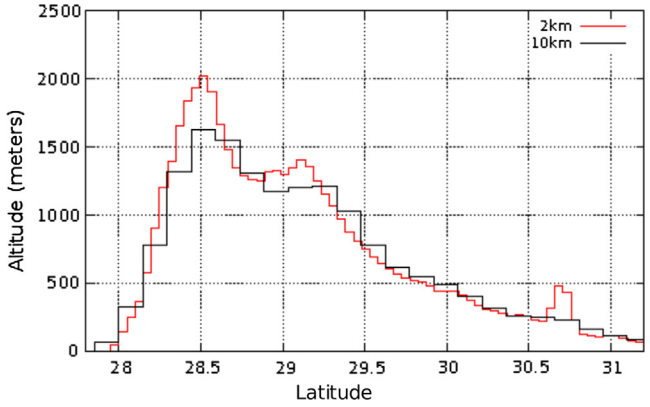

Fig. 15. Representation of Mount Catherine by two different resolutions 10 km (black line) and 2 km (red line).

The atmospheric high resolution modeling is necessary in complex mountainous regions, where the better representation of complex terrain requires small grid distance. Fig. 15 illustrates how two different model resolutions (10 km black line and 2 km red line) represent Mount Catherine (2629 m). Actually both resolutions do not exactly represent the actual mountain features, but the 2-km resolution is better, so the following analysis depends mainly on the 2-km resolution output, in order to capture the topographical effects on the weather.

The synoptic description for this case study is as follows. The upper air charts at 500mb, tell us that during the period from 0 UTC on 12 Feb. to 18 UTC on 13 Feb. there was a ridge over Egypt (see Fig. 16a) and a surface high pressure extended over most of Egypt (Fig. 16b). This situation is associated with stable weather condition. But beginning from 0 UTC 14 Feb, an upper air trough was passing over Egypt from West to East (Fig. 16c), while in the surface there was a deep low pressure over the north coast of Egypt (Fig. 16d). This synoptic situation is the typical unstable weather situation in Egypt's winter, which is known as *Cyprus low* (for more details see El-Fandy, 1946).

The atmospheric condition over South Sinai was stable till the morning of 14 Feb, with clear sky, low relative humidity, and light wind at nighttime, which slightly increased during daytime. During this period, the topography was the main factor in determine the local wind. But in afternoon of 14 Feb, the low pressure began to decrease, wind speed increased, and there were a decrease of temperature (see Fig. 17a) and an increase of relative humidity (see Fig. 17b). With the approaching of upper air trough, the weather became more unstable and during afternoon and evening of 15 Feb the cloud cover increased up to 70% of the sky over Dhalal and 50% over Gunna and St. Catherine airport (Fig. 17c). The rain fell over the region from 19 UTC on 15 Feb till 15 UTC on 16 Feb. with maximum amount around local midnight of 16 Feb (Fig. 17d).

Fig. 17 illustrates the differences of some atmospheric variables (temperature, relative humidity, cloud cover, and rainfall amount) between the two candidate sites and the meteorological station. This figure indicates that during 14 Feb. and 17 Feb. the differences for those atmospheric variables between Dhalal and meteorological station are greater than the difference between Gunna and the station. In another word, during this period Gunna has weather as more similar as that of the airport, while Dhalal has colder temperature, more rainfall, and slightly more relative humidity and cloud.

The prevailing weather condition in the region is resulting from interactions between different scales of atmospheric motions: synoptic, meso-scale, and micro-scale. The synoptic scale motion in winter includes extratropical cyclone and anticyclone, Cyprus low, and Red sea trough, while in summer the synoptic scale includes thermal lows, and in spring season it includes Khamaseen depression. Meso-scale and micro-scale include land-sea interaction, mountain-valley circulation. Fig. 16 gives an example for synoptic scale, while the land-sea interaction is shown in Fig. 18, where there is a wind divergence over relatively cold water surface of Suez Gulf during daytime and there is a wind convergence during nighttime, because the water surface is relatively warmer than land. Also, Fig. 18 illustrates the mountain-valley circulation, where during daytime there are mountainous upslope wind mountains and wind convergence on high land, while during nighttime there are mountainous downslope wind and wind divergence on high land.

The differences of wind field between the two candidate sites and the meteorological station can be illustrated by Fig. 19a, which shows the downslope wind from high mountains to valleys, where the wind is strong in the two candidate sites (blue dots) and it is weak at the airport station. These differences are disappeared or masked when the synoptic scale atmospheric motion is the predominant. For example, Fig. 19b shows that the three sites are affected by a similar magnitude north-east wind.

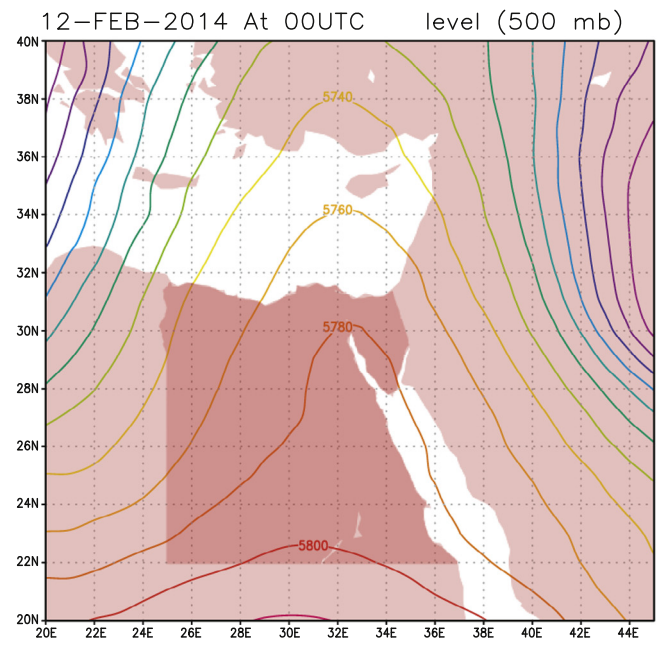

(a) Upper air ridge.

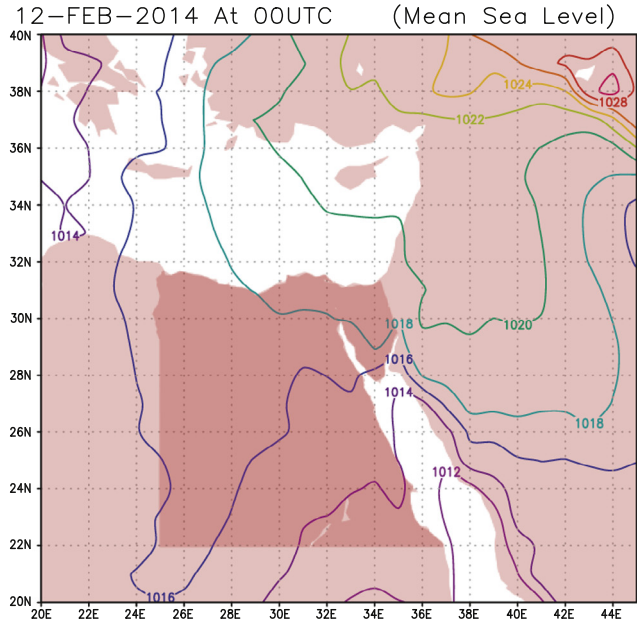

(b) Surface high over most of Egypt

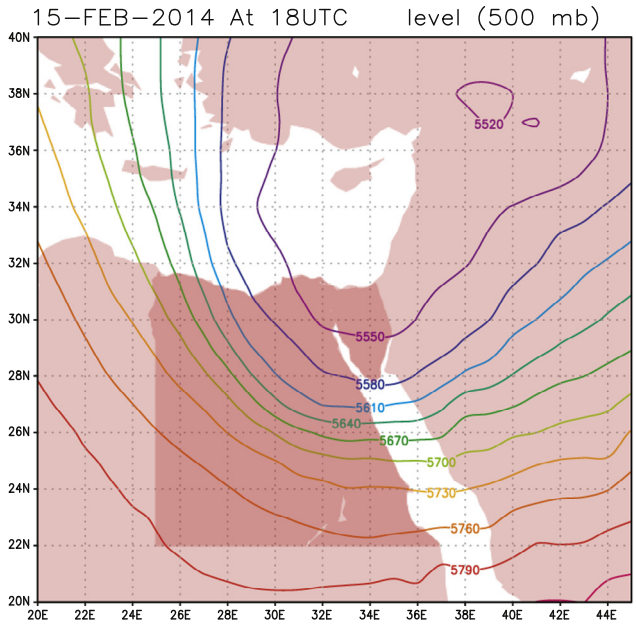

(c) Upper air trough

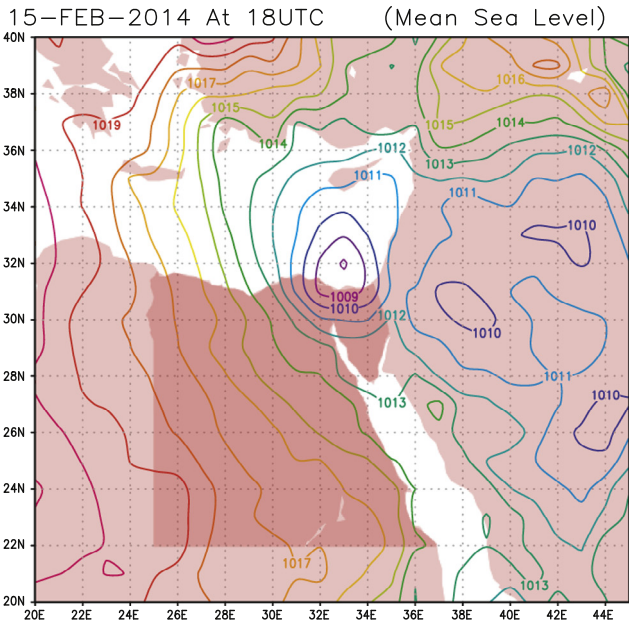

(d) surface low near Sinai coast

Fig. 16. Synoptic situations during stable weather (a and b) and unstable weather (c and d).

The interaction of different scales of atmospheric motion makes a large temporal and spatial variability in the atmospheric flow in the complex terrain region (e.g. see the animation in supplementary material: High Resolution Modeling). Therefore, in order to estimate the operational time of new telescope at the candidate sites based on available climate data from St. Catherine meteorological station, this variability should be taken in account. This can be done by using high resolution modeling for a long period (many years, or at least one year) in order to quantify the variability during all seasons. This will be done in the future work.

Since the case study's simulation indicates that Dhalal site is more affected by the Mediterranean depressions than Gunna and St. Catherine airport, then one can suppose that Dhalal site has more missing hours (nights) in winter than that of Gunna.

11. Estimation for operational nights

The meteorological factors that have bad impacts on the astronomical observations for the candidate sites are discussed in the previous sections, and the associated number of missing nights are calculated. Table 5 summarizes the missing nights for different months under some meteorological conditions.

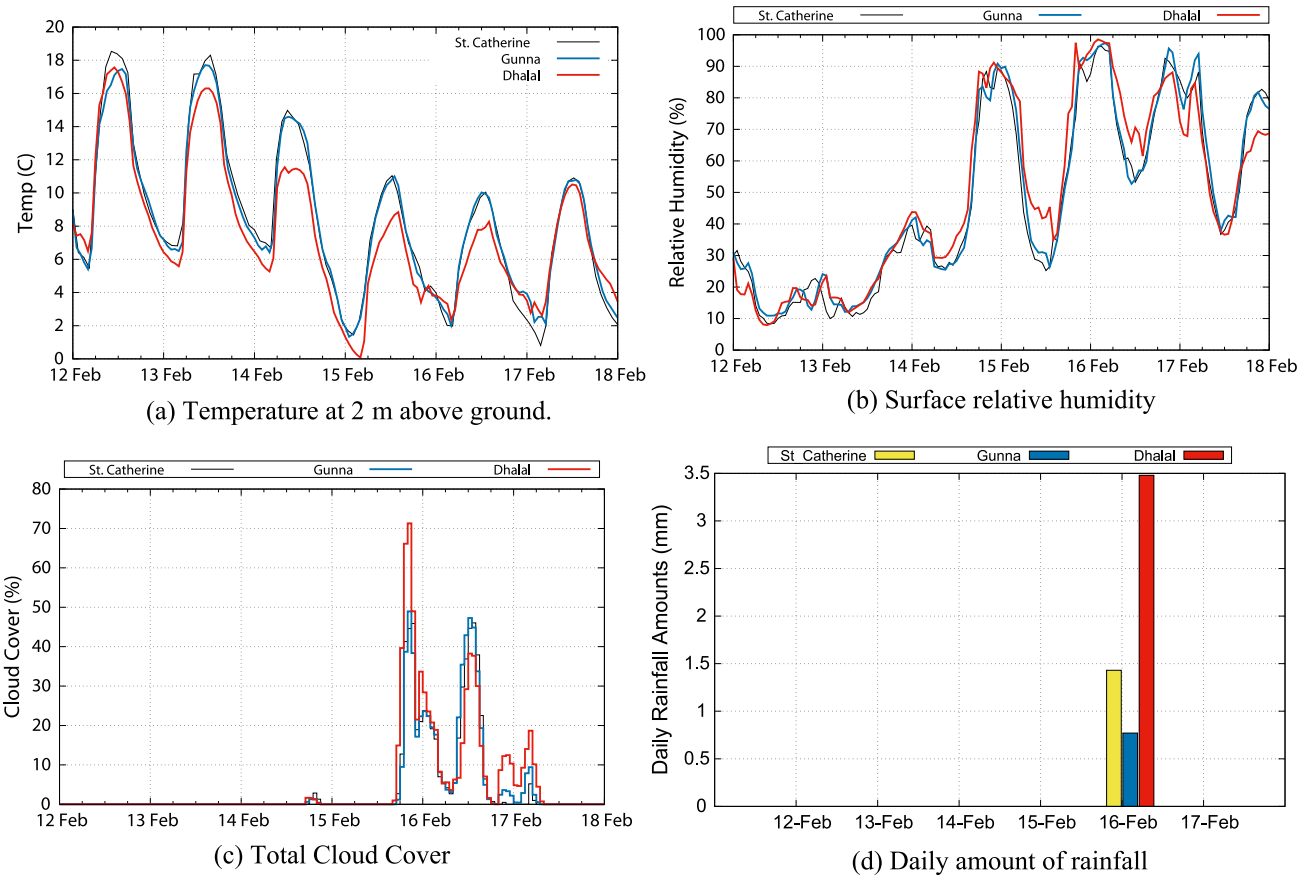

Fig. 17. Comparison of temperature, relative humidity, cloud cover, and rainfall between the three sites (St. Catherine meteorological station and the two candidate sites).

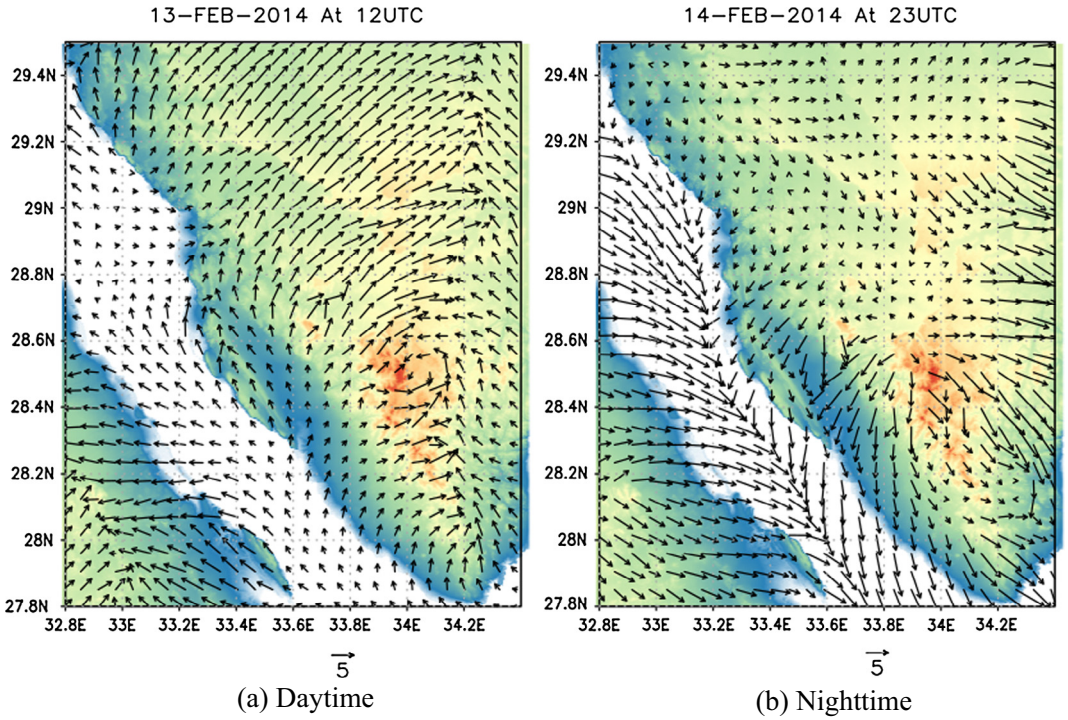

Fig. 18. Land Sea Interaction: during day time, there is wind divergence over Gulf Suez, while during nighttime there is wind converge.

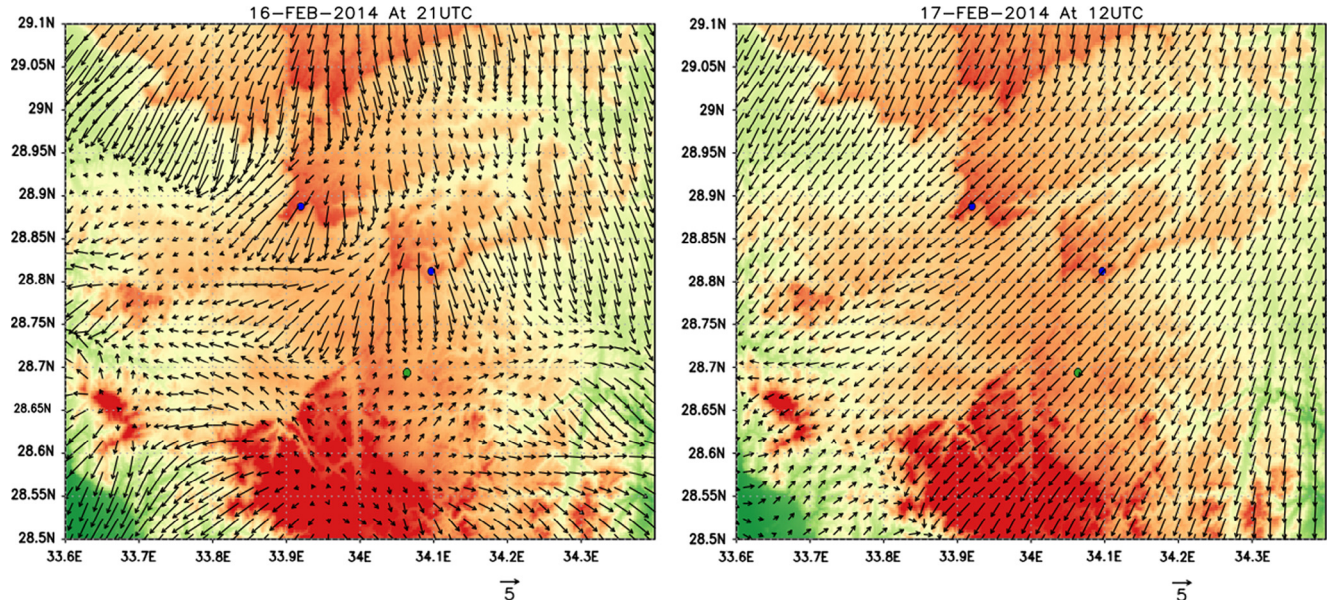

(a) Downslop wind. (b) North east wind.

Fig. 19. High resolution of wind field in candidate sites (see the animation in the supplementary material: High Resolution Modeling).

Table 5
Summary of missing nights under some atmospheric conditions.

Parameter	Jan	Feb	Mar	Apr	May	Jun	Jul	Aug	Sep	Oct	Nov	Dec	Sum
Cloud ≥ 25%	3.0	1.4	1.6	1.5	0.7	0.1	0.4	0.4	0.5	1.0	1.4	1.9	13.9
RH ≥ 75%	10.1	5.2	2.9	0.7	0.6	0.2	0.1	0.2	1.6	2.9	8.6	10.9	43.8
Wind ≥ 15*kt*	2.8	2.2	1.2	0.6	0.8	0.3	0.4	0.2	0.2	0.2	0.2	1.1	10.2
Haze, Sand	0.73	2.47	4.41	4.1	3.73	1.4	0.37	1.27	0.87	1.13	0.37	0.86	21.71
Temp < 0°*C*	7.4	2.0	0.1	0.0	0.0	0.0	0.0	0.0	0.0	0.0	0.0	2.7	12.2

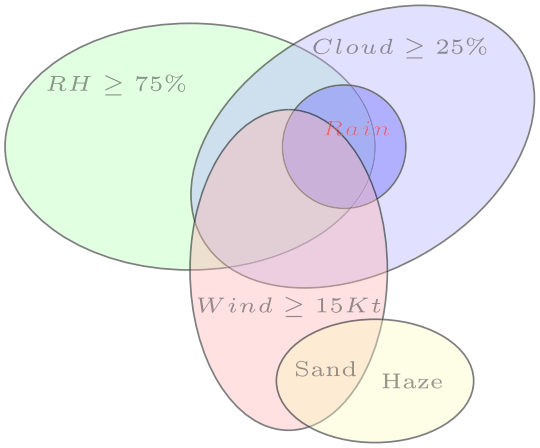

Fig. 20. The intersection between probabilities of atmospheric conditions criteria: cloud cover ⩾ 25%, relative humidity ⩾ %75, wind speed ⩾ 15, rainfall events, sand storm, or raising sand, and haze events.

The summation of all missing nights given in Table 5 will give an overestimation of the actual missing nights, where actually there are intersection between some events (times) that satisfy different criteria. Fig. 20 illustrates the idea of intersection between sets of the probabilities of atmospheric variables that satisfy some criteria. For example, all rain events, P_{rain} intersect with cloud cover condition P_{cloud}, so there is no need to include the missing nights due to rain, where the same nights are already included under cloud cover criterion.

In order to calculate the total number of missing nights as result of all affecting meteorological conditions, we should consider the intersections between these affecting parameters. This can be done mathematically by using probability theory. For example the probability of missing nights as a result of three criteria; cloud cover ⩾ 25%, relative humidity ⩾ 75%, and wind speed ⩾ 15 km/h, can be calculated by using Eq. (1).

$$P_{missing} = P_{cloud} + P_{RH} + P_{Wind} - (P_{cloud} \cap P_{RH}) - (P_{RH} \cap P_{Wind}) - (P_{cloud} \cap P_{Wind}) + (P_{cloud} \cap P_{RH} \cap P_{Wind}) \quad (1)$$

The general formula for the total probability of n arbitrary events with multi-intersection is known as *inclusion-exclusion principle* (Szpankowski, 2001). Which has the following formula:

$$P(E_1 \cup E_2 \cup \cdots \cup E_n) = \sum_{i=1}^{n} \left[(-1)^{i-1} \sum_{J \subset \{1 \cdots n\}} P\left(\cap_{j \in J} E_j \right) \right] \quad (2)$$

By using Eq. (2), the total number of missing hours (day/nights) for different months, by using all available data sets under the following conditions can be obtained.

- cloud cover ⩾ 25%,
- relative humidity ⩾ 75%,
- wind speed ⩾ 15 km/h, and
- temperature ⩽ 0 °C.
- All weather phenomena decrease visibility (Sand, dust, haze, mist).
- All type of precipitation (Rain, Snow, hail, etc.).

The gradient color cells in Table 6 give the missing times (during day and night). Where the probability of best seeing condition

Table 6
No of missing times as results of atmospheric multi-criteria: cloud cover ⩾ 25%, relative humidity ⩾ 75%, wind speed ⩾ 15 km/h, and temperature ⩽ 0 °C.

GMT	Jan	Feb	Mar	Apr	May	Jun	Jul	Aug	Sep	Oct	Nov	Dec	LCT
0	13.3	9.0	7.3	2.6	1.6	0.0	0.0	0.8	2.0	4.4	11.4	14.0	2
1	11.0	8.0	7.0	2.2	2.0	0.6	0.0	0.2	2.8	4.8	11.8	14.2	3
2	11.8	8.5	7.8	2.4	2.8	1.6	1.2	0.6	4.2	6.2	12.0	15.4	4
3	13.0	9.5	7.8	3.8	2.6	1.4	0.8	0.2	5.0	6.2	11.4	14.0	5
4	12.5	8.3	7.0	2.8	1.6	0.6	0.4	0.8	4.2	6.6	11.2	15.2	6
5	11.3	6.8	4.8	2.6	1.2	0.2	0.2	0.0	1.8	4.8	9.2	13.2	7
6	10.0	5.3	4.8	3.4	2.2	1.4	0.4	0.6	1.0	1.8	5.2	10.4	8
7	8.3	4.5	6.0	3.8	3.2	1.2	0.4	0.6	1.6	1.2	3.4	9.8	9
8	8.0	6.3	6.3	6.0	6.4	3.2	0.6	1.4	0.8	2.2	3.8	6.6	10
9	8.8	6.5	6.8	6.8	7.0	3.2	2.4	2.4	3.0	3.4	4.6	6.2	11
10	8.3	6.3	8.3	6.4	9.0	5.8	4.4	4.0	4.2	4.8	5.0	7.0	12
11	8.8	6.5	9.3	8.0	8.8	6.8	5.4	4.0	5.0	6.8	6.6	8.0	13
12	10.8	6.8	11.8	9.4	12.4	9.2	7.6	7.2	6.8	7.4	6.2	7.6	14
13	10.3	7.8	11.8	11.6	12.6	10.6	9.0	8.8	7.2	10.2	7.4	7.6	15
14	9.8	9.5	11.8	12.8	13.6	11.0	8.0	8.4	8.6	10.0	8.0	8.2	16
15	8.5	7.8	10.3	12.2	11.4	11.0	13.0	11.4	8.4	8.2	7.2	6.0	17
16	7.8	6.8	9.5	9.0	10.8	10.2	10.2	10.4	7.4	6.2	5.4	5.8	18
17	8.0	5.0	6.3	8.0	8.2	5.8	7.0	6.0	4.4	3.6	4.4	5.4	19
18	7.8	4.5	4.0	2.8	4.6	2.8	3.2	3.4	2.6	1.6	4.4	6.8	20
19	9.8	4.3	2.8	2.4	3.4	1.2	2.2	1.4	0.4	1.6	5.4	8.2	21
20	10.8	4.5	3.5	2.0	1.8	1.0	0.0	0.4	0.6	2.0	6.4	9.4	22
21	11.0	6.3	4.5	1.4	1.6	0.2	0.4	0.4	1.4	2.0	8.4	10.0	23
22	11.3	6.5	5.5	1.2	1.2	0.0	0.4	0.0	1.4	2.8	9.6	9.8	0
23	12.3	8.3	5.8	2.0	1.2	0.4	0.0	0.4	1.8	4.0	10.2	11.2	1
Night	11.1	7.1	6.0	2.6	2.6	1.2	1.1	1.1	2.4	3.8	9.4	11.6	Sum = 60

occurs in times corresponding to cells have zero or near zero values, while large values with dark colors indicate to more probable missing hours.

In the previous section, it was mentioned that Dhalal site may be more affected by Mediterranean low pressures passing North Egypt than Gunna site and the meteorological station. According to Soliman (1953) the number of these lows is between three and five depressions per months during winter (Nov., Dec., Jan., and Feb.). Therefore, the number of missing nights during winter in Dhalal site may be slightly greater than that of Gunna and that based on St. Catherine meteorological station by 3–5 nights per month during winter.

12. Concluding remarks

The main conclusion of this study is given in Table 6, where the probabilities of missing hours is calculated for each month. This table shows that the total number of missing nights is 60 (i.e. 305 operational nights). This conclusion is based on all available data from St. Catherine meteorological station, that includes the climate normal for thirty years and hourly data for about five years. The meteorological differences between the two candidate sites and the station as discussed in Section 10 suggest that the missing hours in Gunna may be similar to that given in Table 6, while Dhalal site, which may be more affected by the Mediterranean weather, has slightly larger number of missing hours in winter.

This estimation is a preliminary and a more comprehensive study should be done in the future in order to include more advanced analysis and modeling. The following items summarize the missing factors that should be involved in the future studies:

- High resolution modeling for a long period (many years).
- The effect of atmospheric turbulence on seeing.
- Measurements of seeing conditions by using a differential image motion monitor (*DIMM*) at candidate sites.
- Longer period hourly data may give a more robust estimation.
- Study the climate change at the candidate sites.

Acknowledgments

The author is grateful to Professor Magdy Abdel Wahab, Professor Hesham Mousa, and Dr. M. Gabry for their suggestions and comments that improve this study. Special thanks for NRIAG team, who is responsible for choosing the site for the new telescope, for their support and informative advices. Finally, thanks for Egyptian Meteorological Authority (EMA) for providing the data that is used in this work.

Appendix A

See Tables 7–9.

Table 7
Cloud cover frequencies (no of days).

Month	Clear sky or few clouds (< 2/8)	Cloudy sky ⩾6/8
Jan	22.80	0.90
Feb	21.60	0.40
Mar	24.50	0.70
Apr	23.90	0.50
May	26.80	0.40
Jun	29.70	0.00
July	30.60	0.00
Aug	30.80	0.00
Sep	29.40	0.00
Oct	28.40	0.00
Nov	26.10	0.10
Dec	24.50	0.30
Annual	319.10	3.30

Table 8
Mean of cloud cover at 0, 6, 12, 18 UTC.

Month	00 UT	06 UT	12 UT	18 UT	Mean of day
January	1.10	2.00	2.30	1.30	1.60
February	1.00	1.90	2.30	1.20	1.50
March	0.80	1.70	2.10	1.00	1.40
April	0.80	1.50	2.20	1.10	1.30
May	0.70	1.30	1.90	0.80	1.00
June	–	0.80	0.70	0.60	0.20
July	–	0.60	0.70	0.60	0.20
August	–	0.60	0.80	0.50	0.20
September	–	0.70	0.90	0.60	0.30
October	0.70	0.90	1.60	0.70	0.70
November	0.80	1.30	1.90	0.80	1.00
December	0.90	1.90	2.20	1.10	1.40
Annual mean	0.85	1.27	1.63	0.86	0.90

Table 9
The mean number of Mist, Haze, Rising Sand, and Sand storms.

Mon	Mist	Haze	Raising Sand	Sand storms
Jan	0.13	0.20	0.37	0.03
Feb	0.13	0.47	1.80	0.07
Mar	0.17	1.48	2.76	0.00
Apr	0.00	1.23	2.87	0.00
May	0.00	1.20	2.53	0.00
Jun	0.00	0.50	0.90	0.00
Jul	0.00	0.17	0.20	0.00
Aug	0.00	0.77	0.50	0.00
Sep	0.00	0.70	0.17	0.00
Oct	0.13	0.63	0.37	0.00
Nov	0.07	0.17	0.13	0.00
Dec	0.13	0.10	0.63	0.00

Appendix B. Supplementary material

Supplementary data associated with this article can be found, in the online version, at http://dx.doi.org/10.1016/j.nrjag.2017.04.005.

References

Asaad, A.S., Nawar, S., Morcos, A.B., 1982. Bulline of Helwan Institute of Astronomy and Geophysics Series A II.

Barry, R.G., 2008. Mountain Weather and Climate. Cambridge University Press.

Bradley, E.S., Roberts Jr., L.C., Bradford, L.W., Skinner, M.A., Nahrstedt, D.A., Waterson, M.F., Kuhn, J.R., 2006. Characterization of meteorological and seeing conditions at Haleakala. Publ. Astron. Soc. Pacific 118, 172–182. http://dx.doi.org/10.1086/497622 <http://www.jstor.org/stable/10.1086/497622>.

El-Fandy, M.G., 1946. Barometric lows of cyprus. Quart. J. Roy. Meteorol. Soc. 72, 291–306. http://dx.doi.org/10.1002/qj.49707231406.

Erasmus, D.A., 2000. Meteorological conditions and astronomical observing quality ('seeing') at candidate sites for the Southern African Large Telescope. South Afr. J. Sci. 96, 475–482.

Lombardi, G., Zitelli, V., Ortolani, S., 2009. Astroclimatological analysis of ground based observatories. In: Optical Turbulance: Astronomy Meets Meteorology. Imperial College Press, pp. 232–239. http://dx.doi.org/10.1142/9781848164864_002.

Masciadri, E., Sarazin, M., 2009. Optical Turbulence: Astronomy Meets Meteorology. World Scientific.

Masciadri, E., Vernin, J., Bougeault, P., 1999a. 3d mapping of optical turbulence using an atmospheric numerical model: (I) a useful tool for the ground-based astronomy. Astron. Astrophys. Suppl. Ser. 137, 185–202. http://dx.doi.org/10.1051/aas:1999474.

Masciadri, E., Vernin, J., Bougeault, P., 1999b. 3d mapping of optical turbulence using an atmospheric numerical model: (II) first results at Cerro Paranal. Astron. Astrophys. Suppl. Ser. 137, 203–216. http://dx.doi.org/10.1051/aas:1999475.

Nawar, S., Morcos, A.B., Mikhail, J.S., 1995. Light pollution and night sky brightness at the site of Kottamia Observatory. Earth, Moon, Planets 70, 133–141. http://dx.doi.org/10.1007/BF00619457.

NCEP, 2000. NCEP FNL Operational Model Global Tropospheric Analyses, Continuing from July 1999. http://dx.doi.org/10.5065/D6M043C6.

Skamarock, W.C., Klemp, J.B., Dudhia, J., Gill, D.O., Barker, D.M., Wang, W., Powers, J. G., 2008. A Description of the Advanced Research WRF Version 3. Technical Report. <http://www2.mmm.ucar.edu/wrf/users/docs/arw_v3.pdf>. http://dx.doi.org/10.5065/D68S4MVH.

Soliman, K.H., 1953. Rainfall over Egypt. Quart. J. Roy. Meteorol. Soc. 79, 389–397. http://dx.doi.org/10.1002/qj.49707934106.

Stull, R.B., 1988. An Introduction to Boundary Layer Meteorology. Springer.

Szpankowski, W., 2001. Inclusion-exclusion principle. In: Average Case Analysis of Algorithms on Sequences. John Wiley & Sons, Inc., pp. 49–72. http://dx.doi.org/10.1002/9781118032770.ch.

Varela, A.M., Muñoz-Tuñón, C., 2009. Climatology at the roque de los muchachos observatory. In: Optical Turbulance: Astronomy Meets Meteorology. Imperial College Press, pp. 256–263. http://dx.doi.org/10.1142/9781848164864_0030 <http://www.worldscientific.com/doi/abs/10.1142/9781848164864_0030>.

Whiteman, C.D., 2000. Mountain Meteorology: Fundamentals and Applications. Oxford University Press.

WMO, 1975. International Cloud Atlas. Number 407 in WMO Publication, World Meteorological Organization.